16th Australasian Fluid Mechanics Conference
Crown Plaza, Gold Coast, Australia
2-7 December 2007

Oil film interferometry in high Reynolds number turbulent boundary layers

H.C.H. Ng, I. Marusic, J.P. Monty, N. Hutchins and M.S. Chong

Department of Mechanical and Manufacturing Engineering
The University of Melbourne, Victoria, 3010 AUSTRALIA

Abstract

There is continuing debate regarding the validity of skin friction measurements that are dependent on the functional form of the mean velocity profile, for example, the Clauser chart method. This has brought about the need for independent and direct measures of wall shear stress, τ_w. Of the independent methods to measure τ_w, oil film interferometry is the most promising, and it has been extensively used recently at low and moderately high Reynolds number. The technique uses interferometry to measure the thinning rate of an oil film, which is linearly related to the level of shear stress acting on the oil film. In this paper we report on the use of this technique in a high Reynolds number boundary layer up to $R_\theta = 50,000$. Being an independent measure of τ_w, the oil film measurement can be used as a means to validate more conventional techniques, such as the Preston tube and Clauser chart at these high Reynolds numbers. The oil-film measurement is validated by making comparative measurements of τ_w in a large-scale fully-developed channel flow facility where the skin friction is known from the pressure gradient along the channel.

Introduction

The wall shear stress is of great importance in the study of boundary layers. This quantity is especially important because the scaling laws used to describe the velocity profile of a boundary layer, whether that be the logarithmic law or the power law, rely on the wall shear stress, τ_w, to determine the friction velocity in order to non-dimensionalise the velocity term and to define the viscous length scale. Given the density of air, ρ, and the wall shear stress, τ_w, the friction velocity is defined as $U_\tau = \sqrt{\tau_w/\rho}$.

Due to the controversy surrounding the validity of the universal constant terms appearing in logarithmic scaling laws, much more attention is being paid to the accurate measurement of the wall shear stress τ_w. Traditional indirect pressure based methods, such as the Preston tube([12]), rely on the existence of the law of the wall and assumptions regarding the flow field with their accuracy questionable because they are intrusive measures, requiring calibration and corrections, for example, the calibration by Patel [11]. Velocity profile based methods such as the Clauser chart ([1]), are equally limited because it assumes the existence of the law of the wall and requires knowledge of the universal constants *a priori* . Obviously, these methods are unsuitable for determining the validity of the universal laws when they are reliant on their very existence.

The need therefore exists for an unobtrusive, accurate and direct measure of the wall shear stress. Many such methods exist and have been used with varying degrees of success, but each has its own set of limitations which has hindered their widespread acceptance. These techniques include, but are not limited to the wall hot wire, oil film interferometry and the floating element balance. Recent developments in microelectromechanical systems (MEMS) technology has allowed the size of sensors to become increasingly smaller and this avenue shows promise for the development of shear stress sensors. For a more comprehensive review of the available shear stress measurement techniques the reader is directed to work by Winter [20], Fernholz *et al.* [4], Naughton & Sheplak [8], and Ruedi *et al.* [13].

Of the available methods of shear stress measurement, the floating element gauge and oil film interferometer are "direct" measures and require no calibration. Based solely on the thinning rate of a thin oil film and the forces imparted on the film as flow passes over it, the oil film interferometer can be used to obtain the wall shear stress without detailed knowledge or assumptions made about the flow field. The technique is rather robust, in that it can be applied to surfaces with curvature, such as aerofoils, as demonstrated by Driver [3]. It can be applied to flows with adverse pressure gradients and three-dimensional flows and can even be extended to find the direction of the imposed shear stress and used to detect separation and reverse flow. Oil film interferometry is easily set up and the required equipment are all commercially available. The technique does have several major drawbacks, such as contamination of the oil film and uncertainties regarding the properties of the oil which have a major impact on the accuracy of the measurements.

It was first realized by Tanner & Blows [18] that the thinning rate of an oil film, could be applied in a simple relationship, to the measurement of shear stress, by using the thin oil film equation developed by Squire [15]. Tanner [16, 17] and Tanner & Kulkarni [19] continued to develop the technique and further work by Monson [5] and Monson & Higuchi [6] modified and further improved the oil film interferometer. There are many variations of the oil film interferometry technique all of which are based on the original form proposed by Tanner & Blows [18]. These fall into the categories of point, line and image based techniques and included the Laser interferometer skin friction (LISF), Fringe-imaging skin friction (FISF), Global imaging skin friction (GISF) and Surface-imaging skin friction (SISF) methods. A comprehensive review of the various methods is given by Naughton & Sheplak [8]. Over the course of time, the technique has continued to evolve given the advances in image acquisition technology and improvements to the analysis techniques.

Background

Oil film interferometry is based on the relationship between the thinning rate of the oil film and the three forces that may act upon it; gravity, pressure gradient and shear force. When the oil film is sufficiently thin, the effect of gravity and pressure forces becomes negligible, and hence a linear relationship exists between the thinning rate of the oil and the shear force acting upon it. This thickness of the oil film is most easily measured using interferometric techniques.

If a co-ordinate system is defined such that x is the streamwise direction, y the wall normal direction and z the spanwise direction, then the relationship between the oil film gradient and the shear force as first expressed by Tanner & Blows [18] is

$$\frac{dy}{dx} = \frac{\mu_{oil}}{\tau_w t}(1+\varepsilon) \tag{1}$$

where dy/dx is the instantaneous oil film gradient, μ_{oil} is the viscosity of the oil, τ_w the wall shear stress, t is time and ε is the term associated with the effects of pressure gradients and is given by

$$\varepsilon = \frac{1}{3}\frac{y}{\tau_w}\frac{dP}{dx} + \frac{2}{3}\frac{\mu_o il}{t}\int_{p_0}^{p}\frac{1}{{\tau_w}^2}dP. \tag{2}$$

Since the thickness of the oil film is inversely proportional to time, Tanner & Blows [18] surmised that for sufficiently thin films, ε will tend to zero and hence the effect of pressure gradients can be neglected, therefore, when under the assumption of constant shear stress, (1) can be re-written as

$$y = \frac{\mu_{oil} x}{\tau_w t} \tag{3}$$

where, here y is the height of the oil film and x is the streamwise distance from the leading edge of the oil film. Monson & Higuchi [6] and Schülein [14] state that (3) holds so long as the change in shear stress is assumed to be small over the distance that is being measured and as such propose that the difference in the distance from the leading edge for any two points in the streamwise direction is Δx, and hence (3) can be expressed as

$$\Delta y = \frac{\mu_{oil}\Delta x}{\tau_w \Delta t}. \tag{4}$$

Allowing $\Delta y = \Delta h$, where, according to Fernholz *et al.* [4], Δh is the difference in the height of the oil film for consecutive fringes

$$\Delta h = \frac{\lambda}{2\sqrt{{n_{oil}}^2 - {n_{air}}^2 sin^2\theta}} \tag{5}$$

where is λ is the wavelength of the light source (λ = 589.9nm for a sodium lamp), n_{oil} and n_{air} are the refractive indices of the oil and air respectively, and θ is the illumination incidence angle. Hence, by combining (4) and (5), and defining the fringe spacing as some difference in distance relative to the leading edge of the oil film, Δx, the shear stress is obtained by

$$\tau_w = \mu_{oil}\frac{\Delta x}{\Delta t}\frac{2\sqrt{{n_{oil}}^2 - {n_{air}}^2 sin^2\theta}}{\lambda}. \tag{6}$$

Experimental Procedure

Viscosity Measurement

Figure 1 shows the temperature dependence of the oil viscosity. As reported by Zanoun, Durst & Nagib [21], the uncertainties in the oil viscosity had been the predominant cause for inaccuracy, hence, the temperature dependence of the viscosity of the oil needs to be experimentally determined. Dow Corning

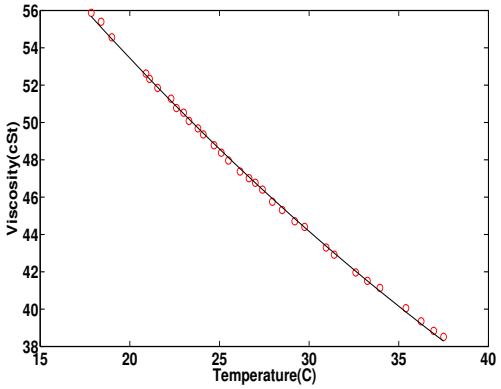

Figure 1: The variation of viscosity with temperature for 50cSt Dow Corning 200 Fluid.

200 Fluid, a silicon based oil can be obtained in many different nominal viscosities, and samples of 50, 100 and 200 cSt oils were obtained. The 50cSt oil was found to be sufficient for the shear stress magnitudes in this study. Silicon oils are preferred because of their chemical stability, and because the viscosity of silicon oils does not vary with temperature as much as that of other oils, however, it is still not negligible. The viscosity of the oil was measured at 32 different temperatures using a capillary viscometer immersed in a constant temperature bath in order to obtain the oil viscosity as a function of temperature. The refractive index and specific gravity of the oil are provided from the manufacturers' data and is assumed invariant with temperature. According to the manufacturer, the viscosity profile of the oil can be modeled using (7).

$$\nu_{oil} = Ae^{-kt} \tag{7}$$

A curve fit was applied and yielded constants of A = 78.24 and k = 0.01906. This relationship provides a satisfactory fit with an error of $\pm 1\%$.

Channel Flow Facility

The experiment was first conducted in a high quality, large scale turbulent channel flow facility, designed and constructed by Monty [7]. The working section measures 0.10m $\times$ 1.17m $\times$ 21.96m. The aspect ratio of 11.7 : 1 and the working section length of 220 channel heights is sufficient to ensure two-dimensional, fully developed flow, as verified by Monty [7]. Under the assumption of *nominally* two-dimensional-fully-developed flow, the wall shear stress is known by simply measuring the pressure drop along the channel. Figure 2 shows the streamwise pressure drop along the channel, with static pressure measurements taken at six streamwise locations, downstream of the sand paper tripped inlet at $x = 7.29, 9.73, 12.17, 14.61, 17.04$ & 19.480m. To obtain the wall shear stress, τ_w, the computed pressure gradient is used in a simple momentum balance applied to a *sufficiently* narrow region encompassing the centreline of the flow, resulting in

$$\tau_w = \frac{h}{2}\left|\frac{dP}{dx}\right| \tag{8}$$

where h is the channel height and $|dP/dx|$ is the pressure gradient. This relationship gives τ_w which is used to validate the accuracy of the oil film interferometry technique.

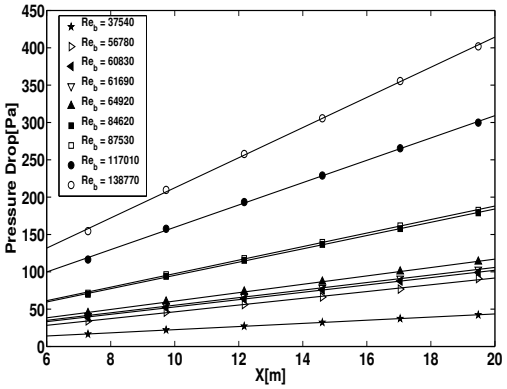

Figure 2: Pressure gradient distribution in the working section of the channel at different Reynolds numbers.

The oil film measurements were conducted at a streamwise location of $x = 205.5 \times H$ from the inlet to ensure fully developed flow. At this location, a circular hole was cut into the channel floor and a matching aluminium plug was machined to fit the circular hole. Many different types of surfaces were tested in order to capture a fringe pattern, with the requirement that the test surface be optically smooth, flat, transparent and partially reflective. Several plastics such as *Mylar* and *Solarfilm* were tried with varying degrees of success. None produced fringes of the quality commonly observed in the literature. For example, the flatness of the surface of the plastics tested were found to be insufficient which caused a strange behaviour of the oil film. The decision to use glass as suggested in the original paper by Tanner & Blows [18], was made for several reasons; the most important being that the surface quality of the glass could be guaranteed, glass is not reactive when cleaned with solvents, does not scratch nor tarnish easily and possesses ideal optical properties producing high quality interferograms. A 3mm thick *Pyrex* glass disc was ground to size, and painted black on the underside in order to maximize the absorption of the transmitted light that was not reflected by the oil film. This was then installed along with the alumnium plug into the channel floor. A 'k type' thermocouple was adhered to the test surface and it is assumed that for a sufficiently thin film, the oil temperature is the same as that of the test surface. Care was taken to ensure that the glass disc was flush with the floor of the channel as the existence of a large enough step or groove would have an influence on the flow and hence a marked effect on the measurements ([9]).

The remaining apparatus consisted of a PCO Pixelfly CCD-camera system, a 105mm A/F Micro Nikkor lens and a sodium lamp. The working distance from the camera lens to the test surface was 300mm and both the camera and light box were mounted above the roof of the channel with optical access to the test surface provided by means of a perspex window. A monochromatic light source is required to produce the fringes required for analysis. The use of a sodium lamp, $\lambda = 589.9$nm was preferred over that of a laser for several reasons: the sodium lamp illuminates a larger area allowing for higher spatial resolution of the interferograms, is optically more powerful than a laser, yet remains portable, with the entire interferometer easily moved between facilities.

Measurements of the shear stress were made over a range of Reynolds numbers from $Re_b = 37,540$ to $Re_b = 138,770$, where $Re_b = U_b H/\nu$ is defined using the full channel height and the bulk velocity. According to Monty [7], the centreline velocity of the channel, U_{cl}, is linearly related to the bulk velocity, U_b by the relationship $U_b = 0.906U_{cl}$, hence, measurements of U_{cl}, the centreline velocity, pressure gradient and interferograms were recorded simultaneously to ensure comparability. Finally, at the end of each session, 2mm square graph paper was placed onto the test surface and imaged so that the resolution of the interferograms could be determined.

Originally, the oil was injected onto the test surface whilst the flow is at the desired test condition, by means of a syringe with access provided by a small hole in the viewing window. This approach was chosen over that of applying the oil onto the test surface with no flow in order to nullify the effect of the facility start-up time, i.e. the time required for the flow to reach the desired test condition. According to Driver [3], the start-up time effects are non-linear and dependent on the particular facility. Other advantages of injecting the oil with the flow at the desired conditions are that it ensures comparability over successive measurements and reduces the likelihood of contaminating the images due to dust. However, analysis of the initial results showed that injecting the oil with the test facility at the desired conditions would introduce a non-linear effect into the oil film because mass is being added to the oil sheet whilst it is experiencing deformation due to the shear stress acting upon it. As a result, the experiments were carried out by first applying the oil to the test surface before turning on the test facility. This introduces a start-up time uncertainty which can be minimized by ensuring that the start up time is small compared to the total run time.

A sample interferogram is shown in figure 3 and the corresponding pixel intensity distribution for a single row in the interferogram is shown in figure 4. Since, the pixel intensity is a periodic signal, determination of the fringe spacing lends itself to Fourier analysis. Thus, an FFT is applied to the pixel intensity signal and the fringe spacing can be obtained from an analysis of the power spectrum. Figure 5 shows the power spectrum corresponding to the intensity signal, where the signal has been zero padded to avoid insufficient resolution about the peak intensity as experienced by Zilliac [22].

Large Boundary Layer Facility

The experimental apparatus is set up in a similar manner in a large boundary layer tunnel. The tunnel is an open return blower type with a rectangular cross sectional area of $0.97\text{m} \times 1.89\text{m}$ and a working section length of 27.00m. Details of the tunnel can be found in Nishizawa, Jones & Chong [10].

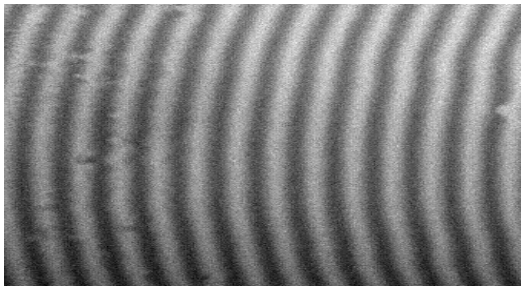

Figure 3: Sample fringe pattern.

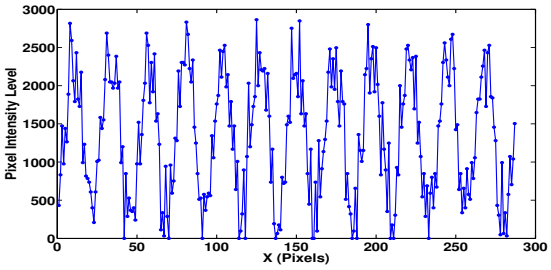

Figure 4: Corresponding streamwise intensity distribution.

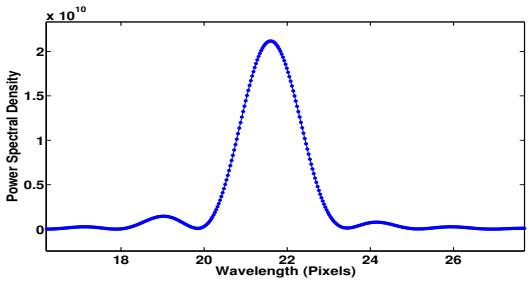

Figure 5: Power Spectrum Density

The boundary layer thickness in this facility is approximately 0.33m. The flow in the working section of interest was verified to be a two-dimensional zero pressure gradient boundary layer. The glass disc and aluminium plug arrangement was installed into the floor of the tunnel at $x = 21.30$m downstream of the sand-paper trip. To allow optical access to the test surface, a perspex window of 0.45m $\times$ 1.20m was constructed and installed as a replacement panel in the ceiling of the tunnel. At this point, the pressure distribution was measured to ensure that installation of the window had not upset the pressure gradient in the working section. Originally, it was planned to have the camera mounted inside the tunnel which was deemed acceptable so long as the camera was at a sufficient distance from the edge of the boundary layer, however, the final arrangement used had both the sodium lamp and camera mounted outside the tunnel to ensure that there would be no flow disturbance whatsoever.

Similar to the channel facility, the oil is deposited onto the test surface before the wind tunnel is started, hence the uncertainty associated with the start up effects remain. The large working distance from the camera to the test surface meant that the spatial resolution of the interferograms is diminished in the boundary layer tunnel when compared to those of the channel, however, good quality signals were still obtained.

Preston tube measurements were made simultaneously to the oil film measurements to ensure comparability. A total head tube of 1mm diameter was attached to the floor of the working section, with great care taken to ensure that the tip of the tube was at the same streamwise location as the oil droplet. The static pressure was measured from a pressure tapping that was aligned with tip of the Preston tube. The pressure measured by the Preston tube was sampled for several minutes to determine the mean skin friction.

Results and Discussion

Channel Flow Facility

The wall shear stress is commonly expressed in a non-dimensional form given by the co-efficient of skin friction

$$C_f = \frac{\tau_w}{\frac{1}{2}\rho U_b^2}. \tag{9}$$

From the definition of friction velocity, $U_\tau = \sqrt{\tau_w/\rho}$, the skin frcition co-efficient in (9) can be expressed as

$$C_f = 2\left[\frac{U_\tau}{U_b}\right]^2. \tag{10}$$

The distribution of skin friction values obtained from both the oil film interferometer and pressure gradient have been plotted alongside the curve fits produced by Dean [2] and Zanoun, Durst & Nagib [21] in figure 6. The variation seen in the skin friction data obtained from the oil film interferometry generally lies within $\pm 2.5\%$ of the skin friction determined from the pressure gradient.

As stated in the previous section, Fourier analysis was used to determine the fringe spacing. To elaborate, if one imagines that the interferogram is a digital image comprised of rows of pixels with each row taken to be perpendicular to the fringes in the interferogram, then each row of pixels will produce a pixel intensity signal resembling a sinusoidal function since fringes are made up of recurrent light and dark bands. An FFT is applied to the signal and the fringe spacing in pixels is determined from wavelength corresponding to the dominant peak of the power spectrum. This process is repeated for each row and then an average taken over the number of rows in the image so that a single wavelength is returned for each image in the sequence. With the scaling of pixels to metres and time interval between images known, this information was used to produce the fringe spacing as a function of time (e.g. figure 9) where the rate of change is used to compute the shear stress. Analysis of the interferograms was carried out using MATLAB, and a simple algorithm was written that automated the process of determining the shear stress.

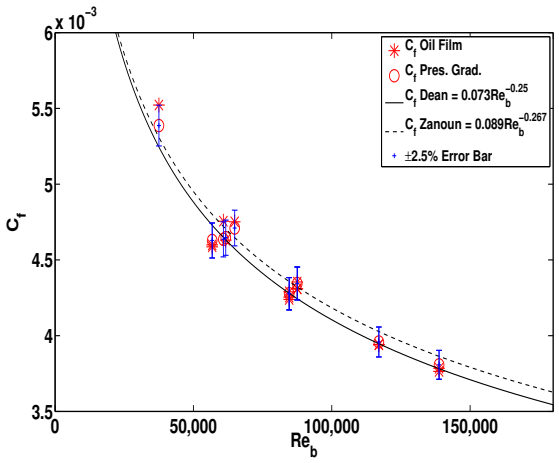

Figure 6: Variation of skin friction as a function of Re_b

Several issues exist when using Fourier analysis to examine the interferograms. One such issue is that of 'pixel locking' due to insufficient resolution about the spectral peaks. This occurs when the wavelength corresponding to the dominant peak in the power spectrum returned by the analysis remains unchanged for consecutive images. This is due to insufficient spatial resolution of the interferogram. This can be rectified by increasing the resolution of the interferograms by using a camera with more digital resolution or even a lens with greater magnification, or by improving the resolution about the spectral peaks by zero-padding the intensity signal prior to applying the FFT. Another potential issue that may arise is that of contamination of the images due to background 'noise'. Great care was taken when preparing the test surface to ensure that background irregularities were kept to a minimum. The analysis is rather sensitive to any background 'noise' in the images and has the effect of causing the power spectrum to have multiple dominant peaks. When the 'noise' overwhelms the signal, the wavelength returned by the analysis may not be indicative of the fringe spacing, but rather the effect of the local noise.

By far the greatest cause of error in the technique is due to contamination of the oil film with dust, and the presence of dust is apparent upon inspection of the interferograms. The effect of dust is twofold. It presents itself as noise in the intensity signal, and also it changes the shape of the fringes as the oil velocity must change when it flowing around the dust particles. This has the effect of changing the wavelength returned from analysis of the power spectrum and hence the measured shear stress.

Ideally, pre-processing steps would ensure that no dust would be caught in the oil film, but this proved extremely difficult as the test facility had to be opened to clean the test surface and also to apply the oil. As a result, a simple filter was devised and incorporated into the algorithm created by the authors to analyze the interferograms. The purpose of this filter was to identify the lines in each interferogram where the power spectrum returned multiple peaks. A threshold value as a proportion of the peak intensity was set and if there existed any secondary peak within this threshold, that line in the interferogram would be discarded in the calculation of the average wavelength. Should the number of lines exhibiting this unwanted behaviour exceed some proportion of the total number of lines making up that particular interferogram, then that interferogram would be removed from the sequence. In this way, the signal-to-noise ratio is increased and any spurious data points removed.

Figure 7 shows a single interferogram taken from a measurement carried out in the channel. Figure 8 shows the wavelength variation across each line in the interferogram, with plots for several different times shown together for comparison. Figure 9 is the corresponding oil film slope history. Each locus of points in figure 8 corresponds to a single image in the sequence and shows the variation in the wavelength across that particular image. The fringe spacing grows over time and hence the wavelength increases. The missing data indicates spurious data points that have been removed by the filter incorporated in the algorithm. Figure 7 corresponds to the top row of points in the plot of the wavelength variation, and clearly, the removed data points in figure 8 correspond the contaminated lines of the interferogram. Figure 9 is the plot of the corresponding fringe spacing as a function of time for the entire run. The gradient of the line is determined to obtain the rate of change of the fringe spacing which in turn yields the shear stress. Figure 8 and

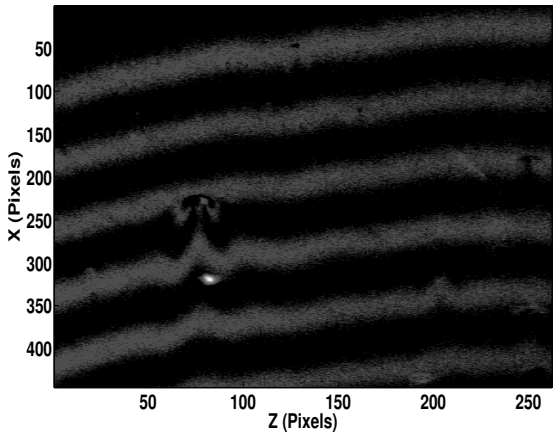

Figure 7: Sample interferogram in channel flow for $Re_b = 64,920$

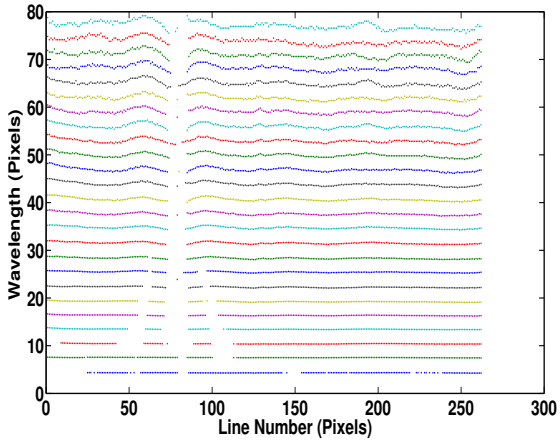

Figure 8: Corresponding peak wavelength variation per line in the interferogram at $Re_b = 64,920$ for certain time intervals.

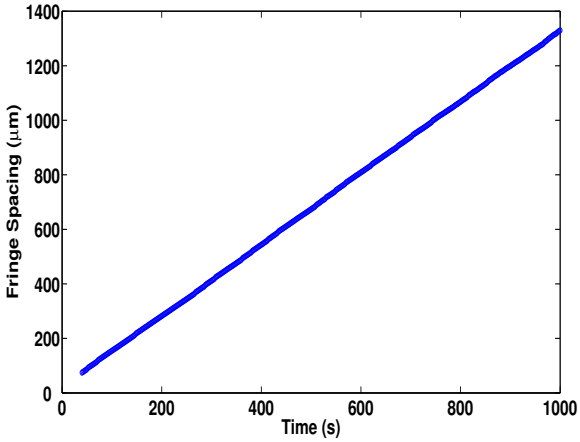

Figure 9: Oil film slope history in channel flow for $Re_b = 64,920$

figure 9 show clearly that the fringe spacing increases linearly over time.

Upon careful inspection, step changes can be seen in the oil film slope history shown in figure 9. These are due to missing images in the sequence of interferograms caused by a buffering problem experienced by the camera, the effect of which is to distort the gradient of the oil film slope history when a straight-line fit is applied to the data. Instead, the difference between adjacent points was determined and the median value returned was used as the gradient to avoid having the magnitude of the shear stress skewed by those discontinuities.

Large boundary layer facility

Shear stress measurements were carried out in the large boundary layer facility at Reynolds numbers of approximately $Re_\theta = 18,500$, $Re_\theta = 35,000$ and $Re_\theta = 50,000$ with Preston tube measurements taken simultaneously to allow comparability. The Reynolds number, is now defined as

$$Re_\theta = \frac{U_\infty \theta}{\nu} \tag{11}$$

where U_∞ is the frestream velocity, θ is the momentum thickness and ν is the kinematic viscosity.

Several minor changes were introduced to the experiment in the large boundary layer tunnel given the findings from the channel. The sampling times were increased substantially because the magnitude of the shear stress acting on the oil had decreased relative to the magnitudes seen in the channel flow, longer sampling times also meant that there would be a decrease in the associated error with the shear stress measurement as verified by Zilliac [22] which is conceivable since the oil film equation only approaches the similarity solution (3) for long times, and finally, long run times meant that any effect of start up transients would be minimized because the time spent in the transient condition would be small compared to the time spent in the test condition. It must noted that *long times* is used in a relative sense because it is dependent on both the oil viscosity and magnitude of the shear stress and also indirectly related to the tunnel start up transient.

Figure 10 and figure 13 show sample interferograms from the large boundary layer tunnel at the two different Reynolds numbers. Both of these interferograms are the last in their respective sequences. Again, the disturbances seen on the film surface are dust particles being caught in the oil film, virtually unavoidable when measuring for extended times. Figure 11 and figure 14 show the variation in the peak wavelength at $Re_\theta = 18,500$ and $Re_\theta = 50,000$ respectively, and figure 12 and figure 15 are the corresponding oil film slope histories. Figure 14 shows a significant variation in the wavelength for increasing time. Early on in the run, there is a linear increase in the wavelength over time even though there is a variation across each image, but as time increases, there is at some point, the onset of non linearity which can be seen in the upper portion of figure 14 where the separation of the plots is no longer consistent. Clearly at $Re_\theta = 50,000$, the peak wavelength ceases to vary in a linear fashion after a certain time, which indicates a breakdown of the oil film.

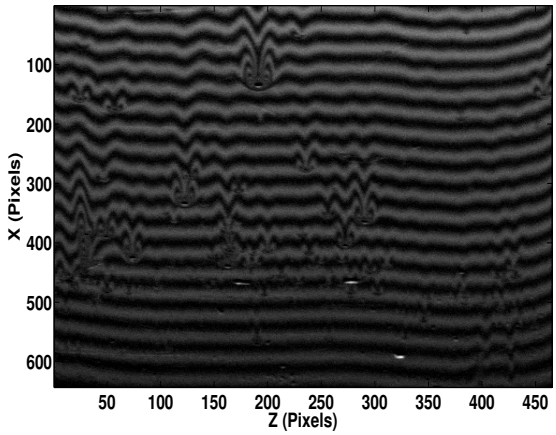

Figure 10: Sample interferogram for large boundary layer tunnel at $Re_\theta = 18,500$.

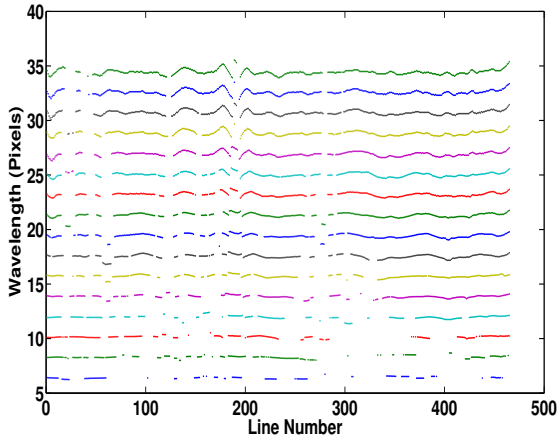

Figure 11: Corresponding peak wavelength variation per line in the interferogram at $Re_\theta = 18,500$ for certain time intervals.

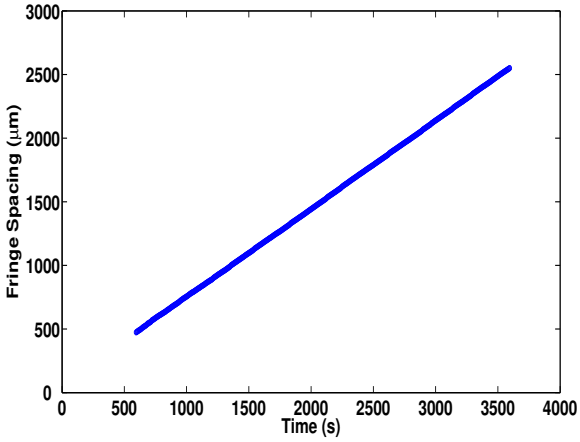

Figure 12: Oil film slope history for $Re_\theta = 18,500$ in large boundary layer facility.

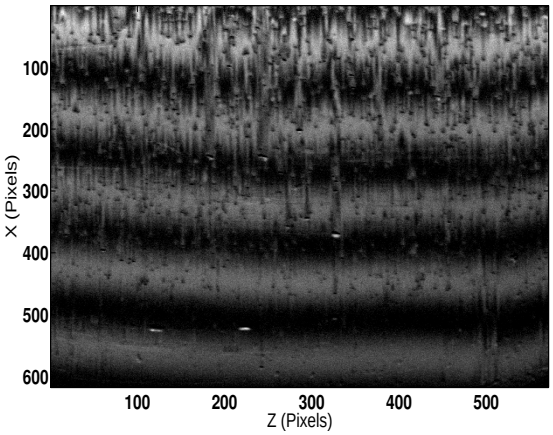

Figure 13: Sample interferogram for large boundary layer tunnel at $Re_\theta = 50,000$.

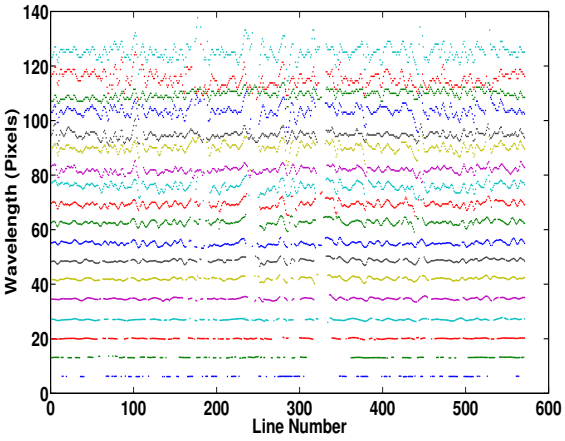

Figure 14: Corresponding peak wavelength variation per line in the interferogram at $Re_\theta = 50,000$ for certain time intervals.

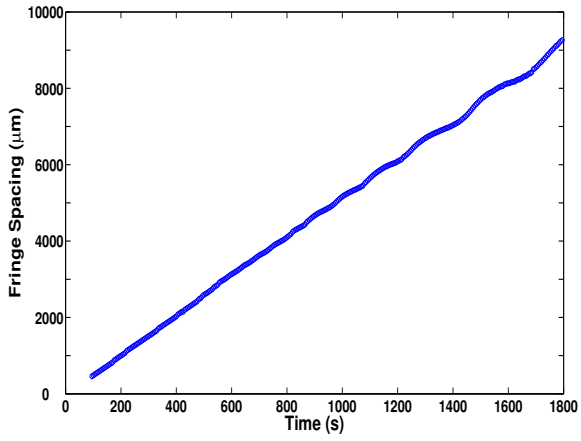

Figure 15: Oil film slope history for $Re_\theta = 50,000$ in large boundary layer tunnel facility

Figure 15 confirms that the oil film has indeed broken down because at times in excess of 1000 seconds, the fringe spacing no longer varies linearly. This duration only applies for this particular combination of oil viscosity and shear stress magnitude, and is not indicative of general oil film break down. The idea that a *long time* in oil film interferometry is a relative concept is clearly illustrated here. Comparing figure 12 and figure 15, it becomes obvious that for this given oil viscosity the definition of a long time can vary from 1000 seconds to more than 3600 seconds, hence, a sufficient run time is determined by the magnitude of the shear stress as well as the nominal viscosity of the oil. Upon examination of the oil film slope histories, it is plain to see that even at these high Reynolds numbers, there is a portion of the slope history which is linear meaning that the theory can be applied within the time bounded by the instant that fringes are first observed and the moment that the variation of the fringe spacing ceases to be linear.

Figure 16 compares the computed skin friction from the oil film interferometry and Preston tube techniques. The measurements from the oil film interferometer and the Preston tube were conducted simultaneously and produced a variation in C_f of no more than $\pm 3.0\%$ for each individual set of simultaneous measurements. There seems to be better convergence between the results obtained from the Preston tube and oil film interferometer at $Re_\theta = 35,000$. However, the skin friction measured using oil film interferometry is consistently higher that that of the Preston tube at $Re_\theta = 18,500$ and then consistently lower at $Re_\theta = 50,000$. This may indicate that there is an optimum range of shear stress magnitudes that an oil of a particular viscosity can measure.

Also, at present, repeatability is questionable because it is very difficult to match flow conditions for successive runs as the tunnel must be powered down to clean the test surface and to apply the oil for the next measurement. As a result, the data plotted in figure 16 must be viewed as individual sets of results between simultaneous measurements using the Preston tube and oil film interferometer and cannot be used to gauge the repeatability of the technique because a method has not yet been devised to exactly match conditions for successive measurements.

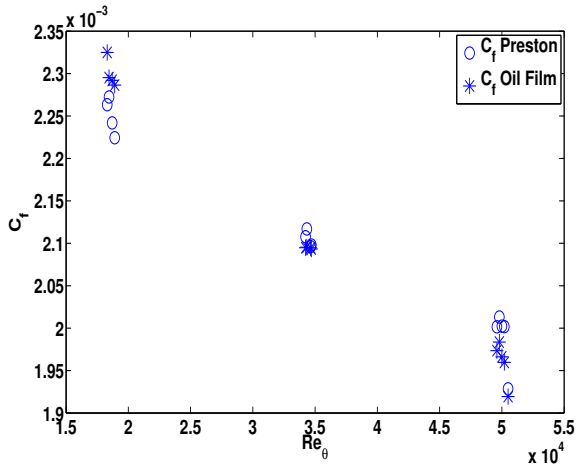

Figure 16: Comparison of skin friction obtained from oil film interferometry to that of the Preston tube.

Conclusions

Oil film interferometry is quite promising and as demonstrated, it is certainly applicable to high Reynolds number turbulent boundary layer flows. For Reynolds numbers ranging from $Re_b = 37,540$ to $Re_b = 138,770$ in the channel flow, τ_w obtained from the oil film technique was found to agree with τ_w obtained from the pressure gradient to within $\pm 2.5\%$. In the boundary layer, τ_w obtained from the oil film technique and the Preston tube were within $\pm 3.0\%$, $\pm 1.5\%$ and $\pm 2.5\%$ of each other, for Reynolds numbers of $Re_\theta = 18,500,\ 35,000$ and $50,000$ respectively.

Further work is being undertaken to address repeatability issues. Also, oils of differing nominal viscosities need to be tested for each Reynolds number in order to determine if there is a range of shear stress magnitudes for which a particular oil is more appropriate, and in the future an innovative method of eliminating the uncertainties caused by tunnel start up transients will need to be developed along with the capability to keep dust particles from contaminating the oil film.

References

[1] Clauser, F. H., Turbulent boundary layers in adverse pressure gradients, *Journal of Aeronautical Sciences*, **21**, 1954, 91–108.

[2] Dean, R. B., Reynolds number dependence of skin friction and other bulk flow variables in two dimensional rectangular duct flow, *Journal of Fluids Engineering*, **100**, 1978, 215–223.

[3] Driver, D. M., Application of oil-film interferomtry skin-friction measurement to large wind tunnels, *Experiments in Fluids*, **34**, 2003, 717–725.

[4] Fernholz, H. H., Janke, G., Schober, M., Wagner, P. M. and Warnack, D., New developments and applications of skin-friction measuring techniques, *Meas. Sci. Technol.*, **7**, 1996, 1396–1409.

[5] Monson, D. J., A nonintrusive laser interferometer method for measurement of skin friction, *Experiments in Fluids*, **1**, 1983, 15–22.

[6] Monson, D. J. and Higuchi, H., Skin friction measurements by a dual-laser-beam interferometer technique, *AIAA Journal*, **19**, 1981, 739–744.

[7] Monty, J. P., *Developments in Smooth Wall Turbulent Duct Flows*, Ph.D. thesis, The University of Melbourne, 2005.

[8] Naughton, J. W. and Sheplak, M., Modern developments in shear-stress measurement, *Progress in Aerospace Sciences*, **38**, 2002, 515–570.

[9] Nishizawa, N., *Measurement of wall shear stress in turbulent boundary layers using an optical interferometry method*, Master's thesis, The University of Melbourne, 1998.

[10] Nishizawa, N., Jones, M. B. and Chong, M. S., A single moduled laser interferometer for wall shear stress measurements, in *14th Australasian Fluids Mechanics Conference*, Adelaide, Australia, 2001.

[11] Patel, V. C., Calibration of the preston tube and limitations on its use in pressure gradients, *Journal of Fluid Mechanics*, **23**, 1965, 185–208.

[12] Preston, J. H., Determination of turbulent skin friction by means of pitot tubes, *Journal of the Royal Aeronautical Society*, **58**, 1954, 109–121.

[13] Ruedi, J. D., Nagib, H., Österlund, J. and Monkewitz, P. A., Evaluation of three techniques for wall-shear measurements in three-dimensional flows, *Experiments in Fluids*, **35**, 2003, 389–396.

[14] Schülein, E., Optical skin friction measurements in the short duration ludwieg tube facility, in *20th International Congress on Instrumentation in Aerospace Simulation Facilities*, 2003.

[15] Squire, L. C., The motion of a thin oil sheet under the steady boundary layer on a body, *Journal of Fluid Mechanics*, **11**, 1961, 161–179.

[16] Tanner, L. H., A comparison of the viscosity balance and preston tube methods of skin friction measurement, *Journal of Physics E: Scientific Instruments*, **10**, 1977, 627–632.

[17] Tanner, L. H., A skin friction meter, using the viscosity balance principle, suitable for use wth flat or curved metal surfaces, *Journal of Physics E: Scientific Instruments*, **10**, 1977, 278–284.

[18] Tanner, L. H. and Blows, L. G., A study of the motion of oil films on the surfaces in air flow, with application to the measurement of skin friction, *Journal of Physics E: Scientific Instruments*, **9**, 1976, 194–202.

[19] Tanner, L. H. and Kulkarni, V. G., The viscosity balance method of skin friction measurement: further developments including applications to three-dimensional flow, *Journal of Physics E: Scientific Instruments*, **9**, 1976, 1114–1121.

[20] Winter, K. G., An outline of the techniques available for the measurement of skin friction in turbulent boundary layers, *Progress in Aerospace Science*, **18**, 1975, 1–57.

[21] Zanoun, E. S., Durst, F. and Nagib, H., Evaluating the law of the wall in two-dimensional fully developed turbulent channel flows, *Physics of Fluids*, **15**, 2003, 3079–3089.

[22] Zilliac, G. G., *Further developments of the Fringe Imaging Skin Friction technique*, NASA Technical Memorandum 110425, 1996.